nature photonics

REVIEW ARTICLE

PUBLISHED ONLINE: 1 MARCH 2017 | DOI: 10.1038/NPHOTON.2017.13

Near-zero refractive index photonics

Iñigo Liberal and Nader Engheta*

Structures with near-zero parameters (for example, media with near-zero relative permittivity and/or relative permeability, and thus a near-zero refractive index) exhibit a number of unique features, such as the decoupling of spatial and temporal field variations, which enable the exploration of qualitatively different wave dynamics. This Review summarizes the underlying principles and salient features, physical realizations and technological potential of these structures. In doing so, we revisit their distinctive impact on multiple optical processes, including scattering, guiding, trapping and emission of light. Their role in emphasizing secondary responses of matter such as nonlinear, non-reciprocal and non-local effects is also discussed.

The control and manipulation of light on the nanoscale — the primary aim of nanophotonics — is of fundamental scientific interest and plays a key role in telecommunication technologies and energy management. Yet, because light–matter interactions are usually weak and hard to confine, they often need to be assisted by the use of suitably designed macroscopic media. For instance, the use of carefully engineered metamaterial structures[1–3] empowers a finer control of light including bending, focusing, filtering, or even its trapping and storage, as well as the realization of all-optical information processing tasks.

Near-zero refractive index photonics — the study of light–matter interactions in the presence of structures with near-zero parameters, that is, continuous media or artificial electromagnetic materials in which one or more of the constitutive parameters are near-zero[1,4–6] (for example, relative permittivity or relative permeability) — exhibits a number of unique features that differentiate it from other material-inspired approaches. In turn, it enables not only unprecedented light–matter interactions, but also the exploration of qualitatively different wave dynamics. According to their predominant electromagnetic response, structures with near-zero parameters at a given frequency can be classified as epsilon-near-zero (ENZ), $\varepsilon \approx 0$, mu-near-zero (MNZ), $\mu \approx 0$, and epsilon-and-mu-near-zero (EMNZ), $\mu \approx 0$ and $\varepsilon \approx 0$ media. All aforementioned classes exhibit a near-zero index of refraction $n = \sqrt{\mu\varepsilon} \approx 0$ at the frequency of interest and can be jointly addressed as zero-index media. A representative sample of different physical realizations of structures exhibiting near-zero parameters is shown in Box. 1.

By simple inspection of time-harmonic source-free Maxwell curl equations, $\nabla \times \mathbf{E} = i\omega\mu\mathbf{H}$ and $\nabla \times \mathbf{H} = -i\omega\varepsilon\mathbf{E}$, for the electric, $\mathbf{E}$, and magnetic, $\mathbf{H}$, fields at radian frequency ω, it is clear that near-zero constitutive parameters ($\varepsilon \approx 0$ and/or $\mu \approx 0$) result in a decoupling of electricity and magnetism, even at a non-zero frequency[1,4–6]. This effect is also accompanied by an enlargement — that is, 'stretching'— of the wavelength, schematically depicted in Fig. 1a, and thus a decoupling of spatial (wavelength) and temporal (frequency) field variations. Consequently, the phase distribution of electric and magnetic fields is necessarily nearly constant in a medium with near-zero permittivity and/or permeability. We emphasize that, far from being a theoretical peculiarity, the connection between wavelength and frequency has a deep technological impact restricting, for example, the size of a device operating at a given frequency and/or the maximal resolution of an imaging device. Thus, 'loosening' the connection between frequency and wavelength in structures with near-zero parameters gives us access to field dynamics relevant from both a fundamental perspective and the possibility of designing unconventional devices.

Ziolkowski's seminal work[4], stimulated by Enoch's proposal of a highly directive antenna[7], was probably the first in-depth analysis of the field dynamics in structures with near-zero parameters. There, it was shown that the fields' spatial distributions in the region with near-zero parameters exhibit a static-like character, even when they continue to dynamically oscillate in time. Naturally, structures with near-zero parameters, as any other physical system, are constrained by causality, and the phase and group velocities associated with these unusual field distributions are discussed in Box. 2. In the remainder of this Review, we examine some of the phenomena originated by the unusual wave dynamics in near-zero photonics, as well as their fundamental and technological implications on different subfields of optics and nanophotonics. We emphasize that although this Review is restricted to photonic structures with a near-zero refractive index, analogous concepts and techniques can be applied to other types of waves, for example, acoustic[8–11] and matter[12–14] waves.

Tunnelling through distorted channels

Arguably, the first theoretical prediction of an exotic wave phenomenon was the tunnelling of electromagnetic waves through a narrow two-dimensional (2D) channel filled with an ENZ medium[5]. As shown in Fig. 1, when a monochromatic electromagnetic wave impinges on a narrow channel filled with an ENZ medium, both the electric field and the power flow are compressed into the channel, and the wave is fully transmitted. It can also be recognized that the phase within the channel is constant, and thus the steady-state transmitted wave exhibits a zero phase advance. Quite remarkably, ENZ tunnelling occurs independently of how sharply the channel is turned or bent; we coined the term 'supercoupling' for this effect[15] and it was first experimentally verified at microwave frequencies by using a waveguide at cut-off to emulate an ENZ medium[16,17] (Fig. 1d). Supercoupling basically emerges from the combination of a constant transverse magnetic field, produced by the enlargement of the wavelength in ENZ media, and the associated reduction of the magnetic flux induced by narrowing the channel, which, in turn, imposes a zero circulation of the electric field and enforces full transmission[5]. Alternatively, one can understand this effect more simply by noting that if a near-zero permittivity dramatically increases the medium impedance ($\eta = \sqrt{\mu/\varepsilon}$), this action can be compensated structurally by narrowing the channel, thus maintaining the impedance-matched device[18].

Following this simple intuition, one can anticipate that if the 2D channel is filled with a MNZ medium, then tunnelling will be

Department of Electrical and Systems Engineering, University of Pennsylvania, Philadelphia, Pennsylvania 19104, USA. *e-mail: engheta@ee.upenn.edu

Box 1 | Structures exhibiting near-zero parameters.

Different realizations of structures with near-zero parameters are shown in Fig. 4. To begin with, various continuous media exhibit near-zero parameters at different frequency ranges (Fig. 4a). For instance, an ENZ behaviour is observed at the plasma frequency of different materials, including potassium[109] (THz frequencies) and polaritonic materials such as silicon carbide[110–113] (mid-infrared frequencies). Doped semiconductors such as transparent conducting oxides (TCOs)[114–116], for example, aluminium-doped zinc oxide (AZO) and ITO, also exhibit a near-zero permittivity at near-infrared frequencies, around the telecom wavelengths ($\lambda \approx 1{,}550$ nm), with the additional advantages of being a CMOS-compatible and tunable platform whose ENZ frequency can be adjusted by controlling the doping level. Topological insulators such as $Bi_{1.5}Sb_{0.5}Te_{1.8}Se_{1.2}$ (BSTS) exhibit an ENZ response at ultraviolet frequencies[117]. Naturally, the performance of continuous ENZ media is ultimately limited by their intrinsic losses[118], although state-of-the-art materials feature relatively low losses such as $\varepsilon(\omega_p) \approx i0.03$–$i0.1$ for SiC[110–113] at $\lambda_p \sim 10.3$ μm and $\varepsilon(\omega_p) \approx i0.2$–$i0.3$ for AZO[114–116] around $\lambda_p \sim 1{,}550$ nm.

Another alternative is to develop metamaterials mimicking the properties of continuous media with near-zero parameters (Fig. 4b). Probably, the first efforts correspond to pioneering works in artificial dielectrics[119–121], which aimed to simulate the properties of plasmas, and were mostly carried out by using waveguides and wire media at microwave frequencies. For example, the effective propagation constant $k_{eff} = k_0\sqrt{1-(\lambda/2h)^2}$ and impedance $Z_{eff} = \eta_0/\sqrt{1-(\lambda/2h)^2}$ of a TE_{10} mode propagating inside a parallel plate waveguide of height h made of PEC walls, indicates that a waveguide at cut-off ($h = \lambda/2$) can be treated as an ENZ medium, at least in terms of describing the propagation of this mode in the middle plane. However, this concept has been further developed[122], enabling the simulation of complex scattering scenarios[122], D-dot wires[45] and EMNZ media[20,21]. Waveguide-based realizations offer structural simplicity and they have even been scaled up to optical frequencies[36].

Wire media[119–121] also exhibit a Drude-like dispersion behaviour, whose ENZ frequency can be tuned by adjusting the radius of and separation between the wires. This structure was later independently rediscovered under the framework of metamaterials[123–126], first as an essential component of double-negative media[127], and then as the precursor of strong non-local response[94]. However, many other metamaterial approaches can also be adopted. For example, stacked layers of two materials characterized by their permittivity (ε_1, ε_2) and thickness (t_1, t_2) can be described by effective permittivity: $\varepsilon_{eff} = (t_1\varepsilon_1 + t_2\varepsilon_2)/(t_1 + t_2)$ for wave propagation with the electric field parallel to the slabs. Therefore, for $\varepsilon_1 > 0$ and $\varepsilon_2 < 0$, by choosing the ratio of thicknesses/permittivities, one can readily realize $\varepsilon_{eff} \approx 0$. This methodology was successfully demonstrated in the visible by using silicon nitride and silver layers[128].

Yet another successful approach is the use of all-dielectric metamaterials. In short, the geometry of high-index dielectric particles can be designed so that the antiresonances of electric and magnetic dipoles (or electric monopole and magnetic dipole for 2D structures) cross zero almost simultaneously, yielding an effective EMNZ media for an array of such particles[129,130]. This effect can also be understood from a photonic crystal perspective, where the EMNZ point is characterized by a Dirac cone at the Γ point[22,131]. In either interpretation, this realization provides a low-loss pathway to implement structures with near-zero parameters at optical frequencies, and even integration into a chip[131]. Other photonic crystals also exhibit properties related to near-zero constitutive parameters. This is the case of zero-$\bar{n}$ gap structures[132,133], that is, a photonic crystal with zero average refractive index, exhibiting a bandgap robust against disorder, angle of incidence and scaling of the elements.

To finalize, it is perhaps the combination of both approaches, continuous and synthetic media (Fig. 4c), which could provide the best opportunities in the development of structures with near-zero parameters. It was found initially that complementing continuous ENZ media with dielectric rods provides the means for obtaining EMNZ media within waveguides and periodic arrays[20,21]. This is part of a very general effect that we coin 'photonic doping' of ENZ media (I.L., A. Mahmoud, Y. Li, B. Edwards and N.E., manuscript in preparation), in which dielectric particles play the role of 'dopants', enabling the control of the effective permeability of an arbitrarily shaped ENZ body, independently of their position in the host.

observed if the height of the channel is substantially increased[19]. As shown in Fig. 1b,c (centre), this intuition is correct, as it has been demonstrated in numerical simulations and experiments, where a microwave waveguide is filled with split-ring resonators to emulate an MNZ medium.

However, the most extreme forms of tunnelling take place in EMNZ waveguides, that is, when both the relative permittivity and the relative permeability of the material filling the 2D waveguide tend to zero at a given frequency. In this case, a zero electric field circulation is imposed by the zero permeability $\mu \approx 0$ and, therefore, the incoming wave is tunnelled through independently of the geometry of the deformation[20] (Fig. 1b,c, right). From a more simplistic perspective, it can be stated that the EMNZ section becomes an electromagnetic 'point'[20], thus seemingly 'directly connecting' the input and output ports and enabling full transmission. Several implementations of EMNZ tunnelling based on waveguides at cut-off filled with dielectric rods[20,21] as well as photonic crystals[22] have been proposed and experimentally verified.

Interestingly, these 2D tunnelling effects can still occur (or be completely inhibited) in the presence of obstacles[20,23,24]. That is to say, if the waveguide section under consideration is not only deformed and sharply bent but also filled with foreign particles. Indeed, both total transmission and total reflection are possible depending on the characteristics of the obstacle[23,24]. For example, ENZ tunnelling is immune to the presence of perfect electric conducting (PEC) obstacles[20]. On the other hand, EMNZ tunnelling of transverse magnetic (electric) modes is extinguished in the presence of perfect magnetic (electric) conducting bodies, as the boundary conditions on these ideal materials quash the constant magnetic (electric) field inducing the tunnelling effect[24]. From a more practical point of view, it is possible to switch from total transmission to total reflection by using a single resonant dielectric inclusion with tunable permittivity[23], thus providing active control of the transmission through a deformed waveguide.

These and other related tunnelling effects are of fundamental interest and have obvious applications in waveguide systems, particularly those to be integrated in a complex environment. Furthermore, and as is thoroughly discussed in this Review, many unique light–matter interactions are triggered by the fields concentrated in such distorted channels.

Emission into the near-zero region

From a historical perspective, the interest in media with near-zero parameters was initially triggered by the possibility of developing highly directive emitters[4,7]. As noted in Enoch's seminal work[7], basic antenna theory implies that the phase and magnitude uniformity associated with an artificially enlarged wavelength directly leads to highly directive beams. This effect is illustrated in Fig. 2a (left), which

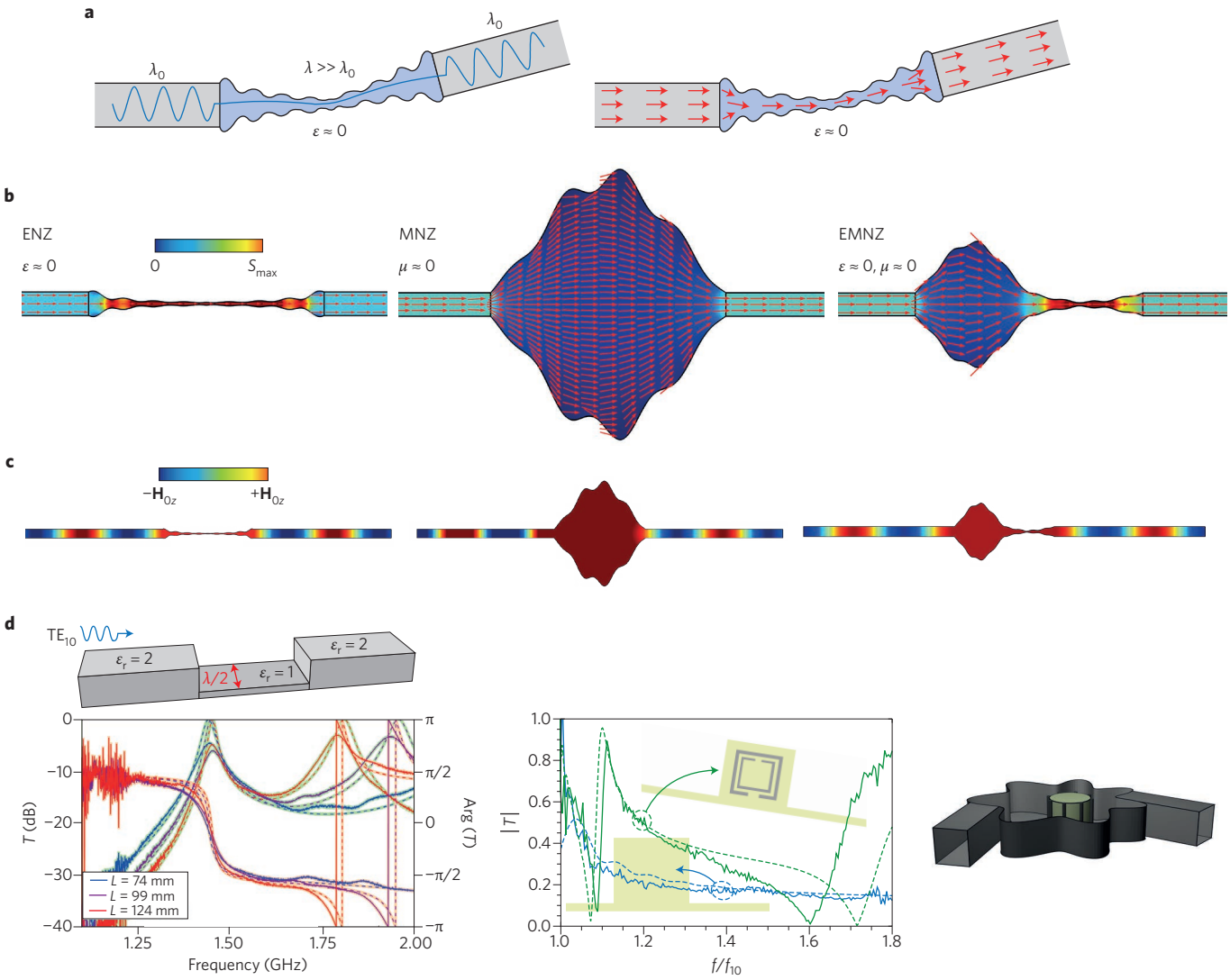

Figure 1 | Tunnelling through distorted channels. a, Conceptual sketch of stretching the wavelength (left) and power flow concentration (right) in waveguide channels filled with media with near-zero parameters. **b**,**c**, Power flow (real part of the Poynting vector field (**b**) normalized to its maximal value S_{max}) and snapshot of the magnetic field $\mathbf{H}_z$ obtained via numerical simulations (**c**; see Methods) for ENZ ($\varepsilon \approx 0$, narrow channel, left), MNZ ($\mu \approx 0$, wide channel, centre) and EMNZ ($\varepsilon \approx 0$ and $\mu \approx 0$, arbitrarily shaped channel, right) supercoupling/tunnelling effects. **d**, Experimental demonstrations of tunnelling, near-unity transmission coefficient T with zero phase advance, in waveguide set-ups. Left: ENZ tunnelling implemented by using a microwave metallic waveguide supporting the TE_{10} mode with cut-off frequency $f_{10} = 1.47$ GHz for relative permittivity $\varepsilon_r = 1$ (see Box I), and revealing full transmission independently of the length of the channel L; centre: MNZ coupling implemented by using a waveguide filled with split-ring resonators; right: sketch of the possible set-up for EMNZ coupling implemented by using a waveguide at cut-off filled with a dielectric rod (experimental results to be reported in a future publication). Figure adapted with permission from: **d** (left), ref. 16, APS; **d** (centre), ref. 19, APS.

depicts the electric field component ($\mathbf{E}_z$) and the radiation pattern excited by a z-oriented 2D current line immersed in an EMNZ cylinder with rectangular cross-section. The current line is insulated from the EMNZ medium by a vacuum circular cylinder. The underlying mechanism behind this highly directive emission can also be understood as spatial filtering. In other words, if the phase is nearly uniform across a straight boundary, only those plane-wave components with near-zero tangential propagation constants will be excited externally to the EMNZ body[7], thus yielding highly directive emission normal to its surface.

In addition to increasing the radiation/emission directivity, the phase and magnitude uniformity can be used for beamforming and beamsteering tasks, that is, for tailoring and reconfiguring the phase and magnitude of the radiation pattern[25]. Indeed, the aforementioned principle empowers a trivial beamshaping technique: the longer one side of the emitter is, the higher the directivity of the beam pointing towards its normal direction. For example, Fig. 2a (right) depicts the emission from an EMNZ cylinder of triangular cross-section, resulting in three radiation lobes, whose directivity scales up with the length of the side. Similarly, as the phase is almost constant within the near-zero structure, an arbitrary phase pattern can be constructed by corrugating its surface[25]. Similar principles can be adopted to arbitrarily shape the phase and magnitude of the scattering pattern and/or for lensing purposes[25].

Several of these theoretical concepts have been implemented in the microwave and millimetre wave frequency ranges. Starting with the first demonstration by Enoch *et al.*[7], involving a monopole antenna radiating within a wire mesh[7], included in Fig. 2b, several metallic ENZ lens antennas have been realized based on extraordinary transmission[26] and tunnelling[27,28]. In the latter, a metallic layer is perforated with waveguides at cut-off. This enables the reconstruction of a wavefront with properties similar to those of an ENZ

Box 2 | Phase velocity and group velocity.

The phase velocity $v_c = c/\sqrt{\mu\varepsilon}$, where c is the speed of light, diverges in media with near-zero parameters ($\varepsilon \to 0$ and/or $\mu \to 0$), resulting in the excitation of static-like field distributions for monochromatic steady-state time-varying fields. Naturally, this quantity does not correspond to the velocity of either energy or information transfer, and structures with near-zero parameters are constrained by causality. Specifically, when a time-harmonic source is switched on, it requires a certain transitory time to reach a steady-state solution for the excited fields. Then, it is in this steady-state regime in which most exotic effects are observed, including, for example, 'static-like' spatial field distributions. Therefore, even if their phase distribution might apparently suggest 'instant' propagation in the steady-state scenarios, the time required to build up this solution ensures that structures with near-zero parameters always comply with causality, and thus the energy velocity is obviously always less than the velocity of light in vacuum. Detailed time-domain analyses of these transitory effects and the convergence towards stationary solutions can be found in the seminal papers[4,134].

In other words, structures with near-zero parameters are necessarily dispersive. Consequently, they always exhibit a finite, sub-c, group velocity, $v_g = \partial\omega/\partial k$, determined by the frequency dispersion of their constitutive parameters. For example, let us consider an ENZ medium characterized by the Drude dispersion model, $\varepsilon(\omega) = 1 - \omega_p^2/\omega(\omega + i\omega_c)$, and $\mu(\omega) = 1$. It is clear that in the lossless limit ($\omega_c \to 0$), the phase velocity diverges at the plasma frequency ω_p, but the group velocity does not. Quite on the contrary, it approaches zero $v_g \to 0$ (refs 80,135), a property of great interest for slow light and nonlinear optics. At the same time, it must be remarked that this result applies only to an unbounded lossless ENZ medium. Therefore, finite-size structures, such as ENZ narrow channels, feature a finite time delay, allowing for the experimental observation of tunnelling effects and the transport of energy through distorted channels.

As another case study, we consider a medium with the same permittivity, $\varepsilon(\omega) = 1 - \omega_p^2/\omega(\omega + i\omega_c)$, but dispersive permeability following the Lorentzian dispersion profile $\mu(\omega) = (\omega^2 - \omega_p^2 + i\gamma\omega)/(\omega^2 - \omega_0^2 + i\gamma\omega)$. This model is representative of several realizations of EMNZ media[20,21]. In this case, the phase velocity again diverges at the plasma frequency in the lossless limit (ω_c, $\gamma \to 0$), but the group velocity is finite and can be written as $v_g = \frac{c}{2}\sqrt{1-\omega_0^2/\omega_p^2}$. Note that, in this case, the group velocity is not necessarily small, and for $\omega_0 << \omega_p$ it quickly converges to $v_g \approx c/2$. This example illustrates that it is, in theory, possible to realize 'static-like' spatial field distributions supporting the propagation of energy and information at velocities comparable to (albeit always less than) the speed of light in vacuum.

obstacle, enabling beamforming, beamsteering[29,30] (for example, see Fig. 2c) and a careful design of the phase front[29,30].

Interestingly, the stretching of the wavelength can also be exploited to enhance collective effects between multiple emitters[20,31–35]. For example, let us consider the emission properties of a collection of fluorescence molecules immersed in a narrow waveguide at cut-off, emulating an ENZ channel. As studied in ref. 31, fluorescence/spontaneous emission is enhanced, even for randomly located molecules, due to two main factors: first, large Purcell factors are induced by the concentration of the electric field in the narrow channel; second, collective in-phase radiation is obtained due to phase uniformity. Indeed, enhanced and position-independent emission in ENZ waveguides was experimentally tested at optical frequencies by exciting a silver waveguide with an electron beam[36]. In passing, we note that the same methodology has been used to propose matched radiofrequency antennas, independently of the position of the probe within the narrow channel[37,38].

Moreover, the highly non-local interactions and collective effects within an ENZ narrow channel might facilitate the observation of Dicke superradiance[32] and spontaneous entanglement generation[34,39]. In the future, we envision that the extreme non-local features and associated collective interactions observed in structures with near-zero parameters might find potential applications in quantum information processing and quantum many-body physics. In addition, the coherence effects associated with non-locality in structures with near-zero parameters might also have implications in other emission processes such as thermal radiation.

Boundary effects and light trapping

One could also anticipate that extreme effects appear at the boundaries of structures with near-zero parameters. For example, note that electric $\mathbf{D} = \varepsilon\mathbf{E}$ and magnetic $\mathbf{B} = \mu\mathbf{H}$ flux densities vanish in ENZ and MNZ media, respectively. Therefore, it is clear that the continuity of their normal components at a boundary, that is, $\hat{\mathbf{n}} \cdot \mathbf{D}$ and $\hat{\mathbf{n}} \cdot \mathbf{B}$, induce strong discontinuities of the normal electric, $\mathbf{E}$, and magnetic, $\mathbf{H}$, fields. A practical application connected to these boundary effects is the possibility of guiding the displacement current, $\mathbf{J}_d = -i\omega\mathbf{D}$, of interest for the development of interconnects for optical metatronics, that is, optical circuits on the nanoscale[40,41]. In essence, if an air groove is carved in an ENZ medium, the displacement current will be zero everywhere except in the air groove, and it will be longitudinal along the boundary within the groove. Therefore, the air groove in the ENZ media, usually referred to as a D-dot wire[42,43], confines and guides the displacement current in a similar way in which conducting wires guide the flow of electrons in an electronic circuit. This simple element could be the basis for constructing all-optical circuit boards on the nanoscale[42]. The operational principle of D-dot wires has been experimentally verified at microwave frequencies with a waveguide set-up[44], and the design of complete waveguide-based displacement current circuits has been proposed[45]. Just recently, an optical wire inspired by D-dot wires was demonstrated in the mid-infrared by using metal–semiconductor waveguides[46].

The inhibition of $\mathbf{D}$ and $\mathbf{B}$ vectors in ENZ and MNZ media, respectively, is in a way a classical and high-frequency analogue of the Meissner effect (complete expulsion of the magnetic field) observed in superconductors. This analogy can be used to extrapolate into optics different effects that are traditionally associated with superconductors. For instance, a scheme for electric levitation, inspired by the levitation of magnets in superconductors, was recently proposed, with the possibility of having repulsive forces more broadband and robust against losses than those of resonant approaches[47].

$\mathbf{D}$ and $\mathbf{B}$ vectors both simultaneously vanish within EMNZ media, conforming the so-called DB boundaries[48,49], that is, a boundary in which both normal electric and magnetic fields vanish in the region external to EMNZ media. Initially, the interest in this sophisticated boundary condition was purely theoretical, aiming to develop electromagnetic equivalence principles, an alternative to the standard formalisms based on the tangential components of the fields. Later on, DB boundaries attracted the attention of researchers in electromagnetic theory due to their unusual scattering properties[50]. Under this perspective, the scattering of EMNZ bodies is of great interest, as they inherit all features of abstract DB boundaries, plus those associated with zero phase advance and 'stretching' of the wavelength within the body.

Another unique feature of structures with near-zero parameters is the possibility to trap and confine light in an open 3D system, in analogy with bound states in the continuum[51,52] and/or

non-radiating modes[53,54]. However, in contrast to other photonic analogues of bound states in the continuum[55,56], a photonic state can be bound to an open, 3D, finite-size body with near-zero parameters, and ideally (in the absence of dissipation losses) remain confined within it for an infinite lifetime. An example of an 'arbitrary' body supporting a bound eigenmode and the associated electric and magnetic field distributions is shown in Fig. 2d. This effect was first identified when studying the emission properties of a small dipole embedded in a spherical plasmonic shell, where zero radiation was consistently observed at the ENZ frequency of the continuous shell[57]. Subsequently, the existence of bound states or embedded eigenvalues in spherical ENZ shells was explicitly derived[58–60] and then generalized to arbitrary (non-spherical) boundaries[35].

Ultimately, the confinement arises as a boundary effect associated with the excitation of time-harmonic spatially 'electrostatic' fields in ENZ media[35]. In short, a time-harmonic but spatially electrostatic electric field $\mathbf{E} = -\nabla V$ (with zero magnetic field $\mathbf{H}$) can be found as the solution to Laplace's equation $\nabla^2 V = 0$, subject to the continuity of the electric potential V and $\varepsilon(\partial V/\partial n)$. By inspecting these boundary conditions, it is clear that the boundary between ENZ and conventional dielectric media behaves as that of a dielectric with a perfect conductor, respectively (note that this is true only for these spatially electrostatic dynamic fields), enabling the existence of a state bound within the ENZ region[35]. Quite remarkably, these bound states exist independently of the geometry of the external boundary, leading to the notion of geometry-invariant resonant cavities[61], that is, resonant cavities whose eigenfrequency is independent of the geometry of the external boundary of the cavity, including changes on its size, shape and topology.

It is important to remark that the physical mechanism underlying this geometry invariance is the decoupling between temporal and spatial field variations in structures with near-zero parameters[61]. In other words, the boundedness or non-radiating properties of the modes are not essential to achieve geometry invariance. In fact, there are other families of geometry-invariant eigemodes that do not correspond to bound states. For example, it was also found that transverse magnetic modes in 2D ENZ cavities containing a dielectric rod support eigenmodes whose eigenfrequency is immune with respect to equi-areal transformations of the ENZ region[61]. That is to say, the external boundary of the resonator can be deformed, while preserving the overall area of the device, without changing its resonance frequency[61]. However, in this case, the transversal magnetic field in the ENZ region is different from zero[61]. Consequently, these modes are radiating, and they strongly interact with the environment if PEC walls bounding the cavities are removed.

Both bound and radiating geometry-invariant eigenmodes are the basis of truly exotic resonators, unique to structures with near-zero parameters. We expect that their future development might find applications in flexible and reconfigurable photonic systems, perhaps opening the way to deformable optical resonant devices. Moreover, unique light–matter interactions taking place while deforming the cavity might lead to the observation of new dynamical light–matter bound states in cavity quantum electrodynamics and cavity optomechanics.

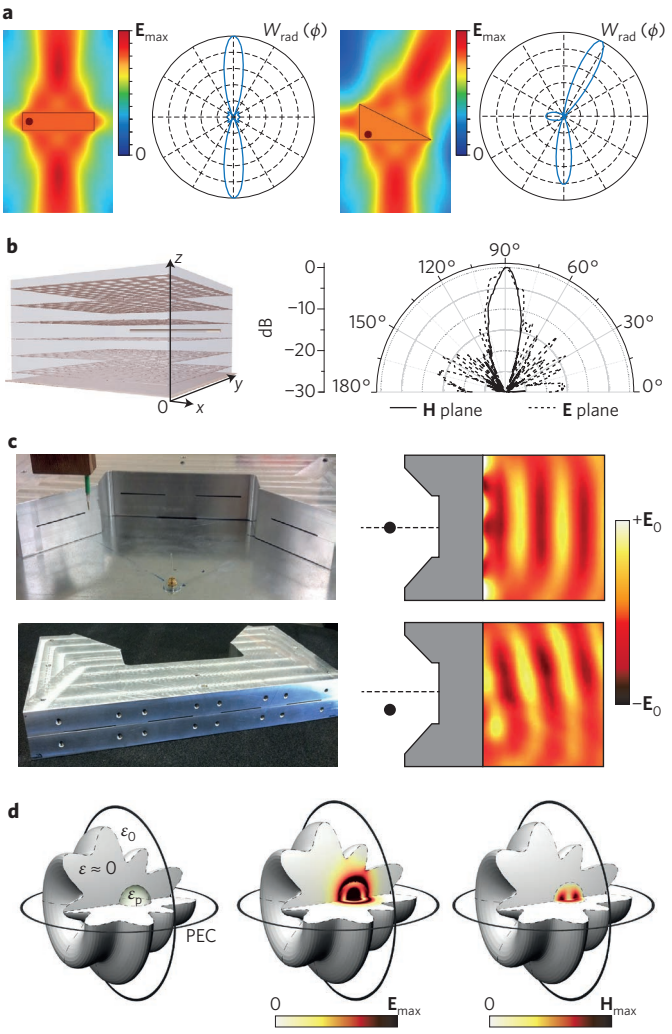

Figure 2 | Highly directive emission and geometry-invariant phenomena. **a**, Numerical simulations (see Methods) of the 2D electric field magnitude, $|\mathbf{E}_z|$, and normalized radiation intensity, $W_{rad}(\phi) = \frac{1}{2}\mathrm{Re}\{\mathbf{E} \times \mathbf{H}^*\}$, excited by an insulated 2D current line source immersed in 2D EMNZ cylinders of rectangular and triangular cross-sections. The current line is insulated from the EMNZ medium by a vacuum circular cylinder. Highly directive beams are generated perpendicular to the sides of the EMNZ body. **b**, Experimental realization and measured radiation pattern based on a wire mesh fed by a monopole antenna at GHz frequencies. **c**, ENZ metallic lens (implemented as waveguides at cut-off) and measured electric field distribution, evidencing high directivity (centred case, top) and beamforming (displaced case, bottom). **d**, Sketch and numerical prediction (see Methods) of the electric and magnetic field distributions for 3D 'open' ENZ cavities containing a dielectric particle of relative permittivity ε_p and supporting a bound (non-radiating or embedded) eigenmode, independently of the geometry of the external boundary, which is touching the vacuum. Figure adapted with permission from: **b**, ref. 7, APS; **c**, ref. 30, IEEE.

Boosting nonlinear optics

Structures with near-zero parameters have a particular synergy with nonlinear optical processes. In fact, near-zero parameters empower two of the main requirements to boost the (usually weak) nonlinear response of matter: phase matching and high field intensities.

On the one hand, phase matching is essential to prevent destructive interference in the fields generated by nonlinear polarization sources. In practice, phase matching is attained with several techniques including birefringent phase matching, angle phase matching and quasi-phase matching[62,63]. Each of these techniques has its own advantages and limitations (see, for example, refs 62,63 for an introduction to phase-matching techniques), but a common characteristic is that they are all limited to provide phase matching in a specific direction[64]. In contrast, the need of phase matching is eliminated in structures with near-zero parameters. There, as schematically depicted in Fig. 3a, the lack of phase progression allows for the fields to build up coherently[64]. This strategy has been demonstrated by enhancing four-wave mixing (FWM) at near-infrared frequencies using fishnet metamaterials featuring a zero-index response[64]. As anticipated, the matching is direction independent, and the generated FWM was successfully measured in both the forward

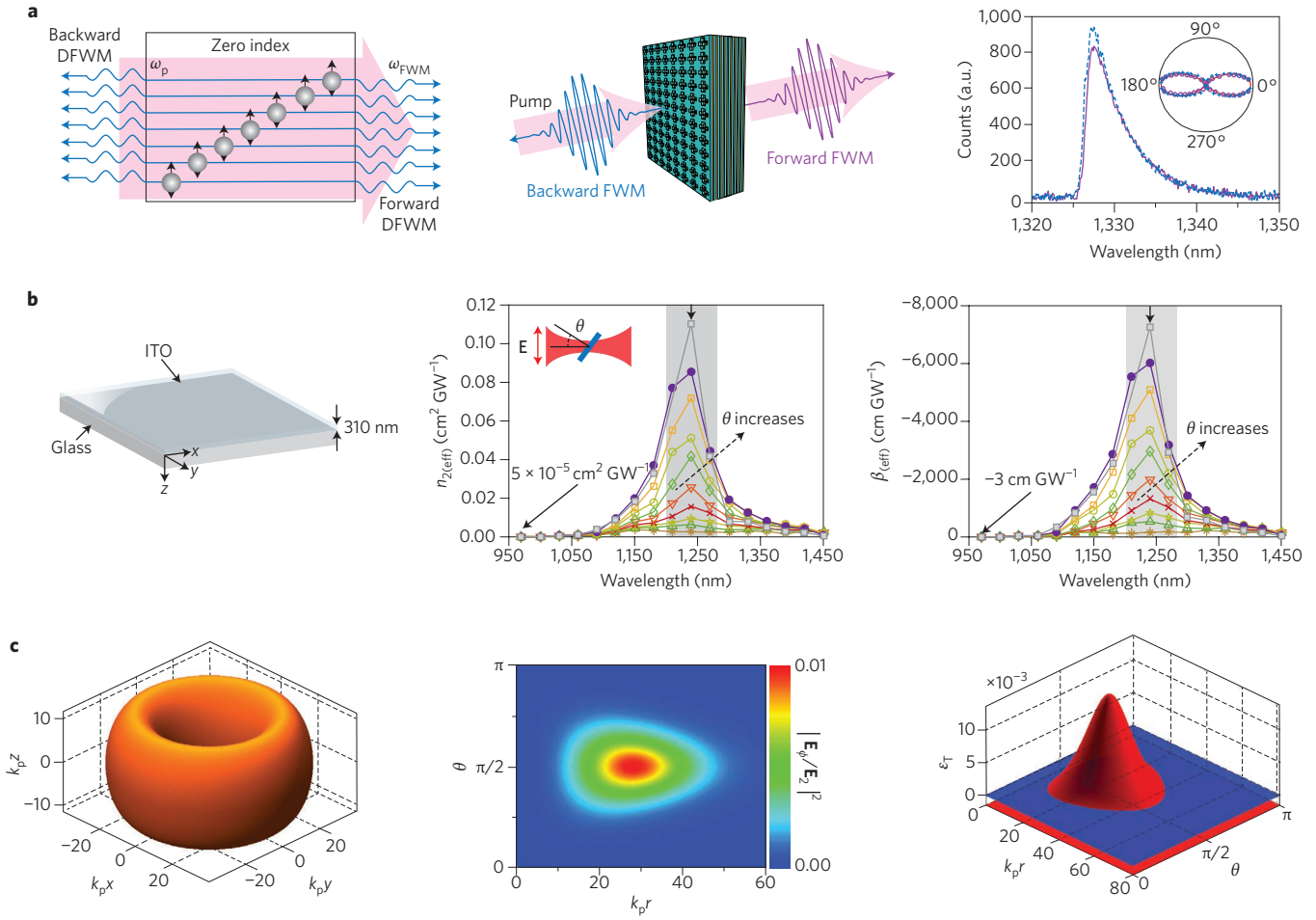

Figure 3 | Nonlinear phenomena in structures with near-zero parameters. a, Phase matching in zero-index media leading to efficient four-wave mixing (FWM) in both the forward and backward directions. DFWM, degenerate four-wave mixing. Sketch (left), geometry (centre) and measured data (right) of the experimental realization with a fishnet metamaterial at near-infrared frequencies. The measured FWM signal in the forward (purple) and backward (blue) directions are shown (right). **b**, Strong nonlinear response in ENZ thin films. Measured nonlinear effective refractive index, $n_{2(eff)}$, and effective nonlinear attenuation constant, $\beta_{(eff)}$, of an ITO film of 310 nm thickness. The ENZ point $\varepsilon'(\lambda_p) \approx 0$ occurs at $\lambda_p \approx 1{,}240$ nm, centre of the shaded region). **c**, Frozen light. Self-sustained 3D confinement of light in an ENZ medium with Kerr nonlinearity. Electric field iso-surface (left) and intensity distribution (centre) as well as dielectric permittivity profile (right) are shown. Blue plane (right) corresponds to the zero-permittivity points. All positions normalized with respect to the inverse of the wavevector at the plasma frequency k_p^{-1}. Figure adapted with permission from: **a**, ref. 64, AAAS; **b**, ref. 71, AAAS; **c**, ref. 85, under a Creative Commons licence (http://creativecommons.org/licenses/by/4.0/).

and backward directions (Fig. 3a). Naturally, this concept is platform independent and it can be easily adapted to other nonlinear processes, and to other platforms with near-zero parameters. This includes, for example, a proposal for phase matching and efficient second-harmonic generation based on photonic crystals exhibiting a near-zero response[65].

However, nonlinear processes are observed only at high field intensities, as the exciting electric fields have to compete with the restoring forces of strong atomic fields. Typically, the field intensity can be increased by concentrating it in a small region of space, for example, by using nanoantennas. In stark contrast, structures with near-zero parameters can provide large field intensity enhancements over large regions, while simultaneously providing phase matching. This is the case, for example, in narrow channels exhibiting ENZ tunnelling. As shown in Fig. 1c, large field intensities (with the field enhancement being proportional to the ratio between the waveguide heights of the narrow channel and the input waveguide) are uniformly supported along the narrow channel, while exhibiting a zero phase progression that empowers phase matching[66]. A planar optical device exploiting this convenient field distribution could consist of a metallic screen hosting waveguides at cut-off carved with a nonlinear material[67,68]. Preliminary numerical studies suggest that this device could exhibit enhanced Kerr nonlinearities, achieving switching and a bistable response[67], as well as giant second-harmonic generation[68].

In addition, recent experimental efforts have demonstrated that nonlinear effects are strongly enhanced in simple ENZ thin films[69–72] (for example, see Fig. 3b). The reasons behind why such a simple geometry can provide a strong nonlinear response are twofold: first, it can be readily checked that the variation in the refractive index for a given permittivity variation, $\Delta n = \Delta\varepsilon/(2\sqrt{\varepsilon})$, is maximized in materials with near-zero permittivity[71,72]; second, the strong boundary effects, related to the continuity of $\hat{\mathbf{n}} \cdot \mathbf{D}$, ensure that a strong longitudinal electric field (normal to the interface) is induced when the film is illuminated from an oblique angle of incidence[69,70,73]. These works have demonstrated ultrafast and large-intensity refractive index modulation[71,72], as well as second[70]- and third[69]-harmonic generation, two orders of magnitude larger than crystalline silicon. On top of that, the materials employed to provide an ENZ response (for example, indium tin oxide, ITO) are complementary metal-oxide–semiconductor (CMOS)-compatible. Therefore, these results suggest that ENZ thin films might become a key element in nonlinear flat optics in the near future.

ENZ thin films are also receiving interest due to their ability to support the so-called ENZ modes[74–76], that is, long-range surface plasmon polaritons whose dispersion relation becomes ultraflat at the ENZ point as the thickness of the thin-film tends to zero[76]. In turn, ENZ modes allow for enhancing the interaction with metamaterial and semiconductor structures, phonon excitation and thermal emission[75,77–79]. It can thus be concluded that light–matter interactions in ENZ thin films, albeit structurally simple, are significantly rich.

At the same time, nonlinear processes are also strengthened within a bulk ENZ medium. These effects benefit from a low group velocity[80] (see Box 2) and the fact that the nonlinear polarization becomes comparable to the linear polarization[81]. Quite intuitively, low group velocities increase interaction times, and are often accompanied by pulse compression and enhanced field intensity. Therefore, they naturally enhance light–matter and effective photon–photon interactions, which can be exploited in a variety of nonlinear processes[82,83]. Furthermore, the ENZ point is at the transition between an opaque ($\varepsilon < 0$) and transparent ($\varepsilon > 0$) medium, and it is arguably the optimal point to investigate self-trapping and self-organization mechanisms. Indeed, it has been identified that ENZ media support the propagation of two-peaked and flat-top solitons[84]. Moreover, Fig. 3c depicts a static but particularly extreme form of self-organization. In this case, the light does not propagate within the nonlinear media as a soliton, but it is fully confined (self-trapped) in a 3D region with a doughnut-like shape[85]. Owing to the cubic nonlinearity of the medium, the field imprints its own ($\varepsilon > 0$) cavity, within an otherwise opaque ($\varepsilon < 0$) medium.

Exploiting non-reciprocal and non-local responses of matter

Nullifying the predominant response of matter (that is, a linear and isotropic polarization process described by scalar permittivity and permeability) also serves to emphasize secondary responses such as non-reciprocal and non-local effects. Moreover, not only are these effects emphasized, but different wave dynamics appear as permittivity and/or permeability tend to zero. For example, if we consider chiral coupling, κ, in EMNZ media, $\mathbf{D} = i\kappa\sqrt{\mu_0\varepsilon_0}\,\mathbf{H}$ and $\mathbf{B} = -i\kappa\sqrt{\mu_0\varepsilon_0}\,\mathbf{E}$, usually referred to as chiral nihility[86], results in double refraction, that is, the excitation of two waves, exhibiting positive and negative refraction.

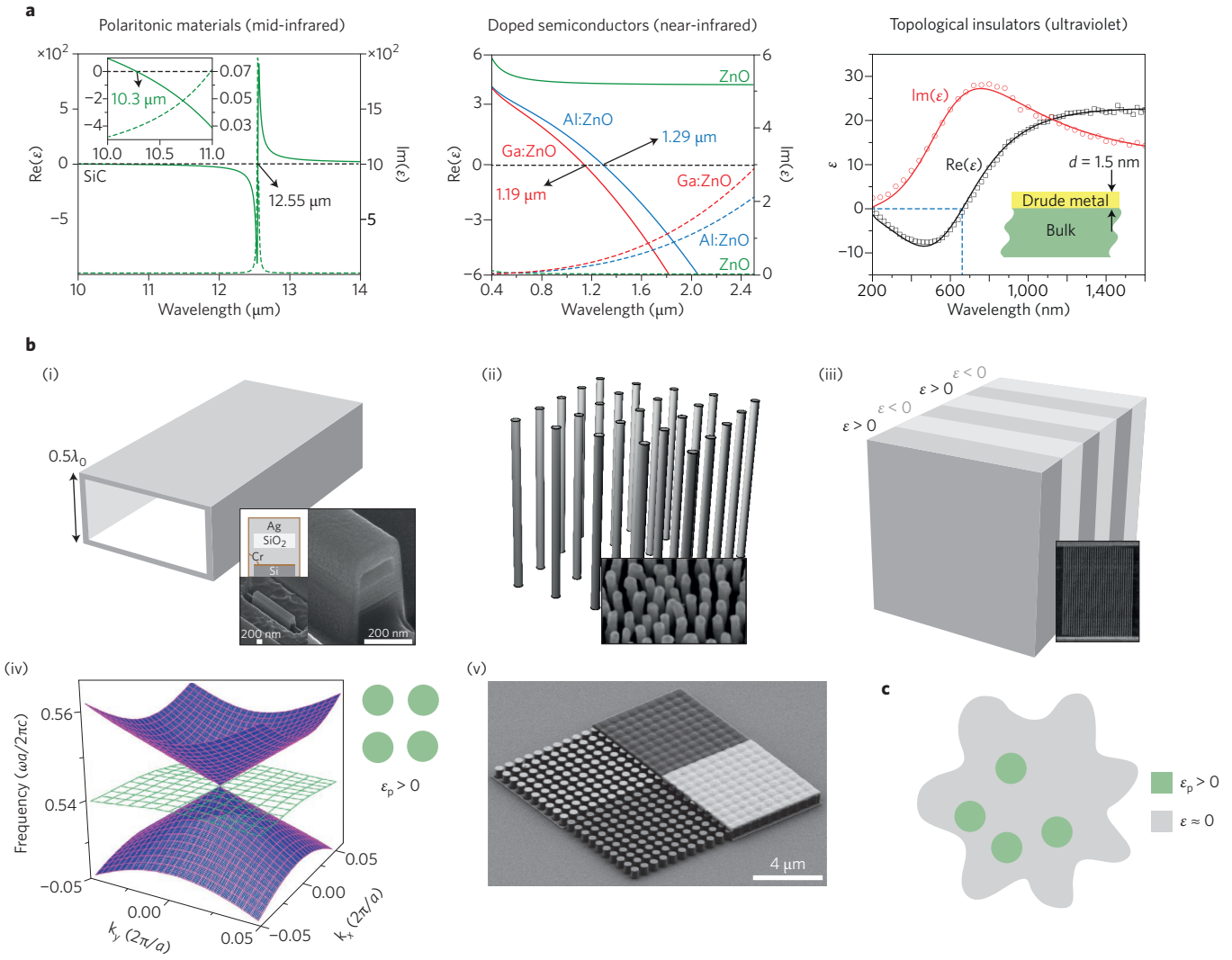

Figure 4 | Different realizations of structures with near-zero parameters. a, Continuous media including polaritonic materials such as SiC at mid-infrared frequencies (left), doped semiconductors such as transparent conducting oxides (TCOs) at near-infrared frequencies (centre) and topological insulators such as $Bi_{1.5}Sb_{0.5}Te_{1.8}Se_{1.2}$ (BSTS) at ultraviolet frequencies (right). **b**, Synthetic implementations including waveguides at cut-off (i), wire media (ii), multilayered structures (iii), arrays of dielectric rods (iv) and/or photonic crystals (v). **c**, Hybrid implementation of continuous and synthetic media such as dielectric particles immersed in a continuous ENZ medium. Figure adapted with permission from: **a** (left and centre), ref. 113, OSA; **a** (right), ref. 117, Macmillan Publishers Ltd.; **b** (i, SEM inset), ref. 36, APS; **b** (ii, SEM inset), ref. 95, APS; **b** (iii, SEM inset), ref. 128, Macmillan Publishers Ltd.; **b** (iv), ref. 22, Macmillan Publishers Ltd.; **b** (v), ref. 131, Macmillan Publishers Ltd.

For magneto-optical media, for example, $\bar{\bar{\varepsilon}} = \varepsilon_{mo}(\hat{\mathbf{x}}\hat{\mathbf{x}} + \hat{\mathbf{y}}\hat{\mathbf{y}}) - i\alpha(\hat{\mathbf{x}}\hat{\mathbf{y}} - \hat{\mathbf{y}}\hat{\mathbf{x}}) + \varepsilon_{\perp}\hat{\mathbf{z}}\hat{\mathbf{z}}$, with α being the off-diagonal element associated with the magneto-optical activity of the media, the use of structures with near-zero parameters (in this case, $\varepsilon_{mo} \to 0$) enables the exploration of new regimes in which $|\alpha/\varepsilon_{mo}| > 1$, by contrast with the usual $|\alpha/\varepsilon_{mo}| << 1$ limit that results from the inherent weakness of magneto-optical activity[87]. In turn, this empowers alternative propagation schemes, including Hall transparency ($-|\alpha| < \varepsilon_{mo} < 0$) and Hall opacity ($0 < \varepsilon_{mo} < |\alpha|$) for transverse magnetic waves in the Voigt configuration[87]. When applied to surface waves, these regimes enable the excitation of one-way surface waves that are protected against backscattering from obstacles[87], with properties similar to configurations based on topological photonics[88–92]. Another interesting feature appears in the case of waves propagating along the magnetization direction. In this configuration, it is found that circularly polarized waves of the same handedness, but opposite directions of propagation, feel the medium as opaque and transparent, with evident applications in the development of compact optical isolators[93]. These results indicate the potential of structures with near-zero parameters in emphasizing and exploiting the non-reciprocal and bianisotropic responses of matter, which are usually hidden behind the predominant polarization process.

An analogous effect occurs with the non-local properties of matter, that is, the induction of polarization that depends on the fields at a different point of space (albeit satisfying causality). For time-harmonic fields decomposed into a basis of plane-waves, this response can be described via constitutive parameters depending on the wavevector, $\varepsilon = \varepsilon_{local} + \varepsilon_{nl}(\boldsymbol{\kappa})$, and media with a substantial non-local response is said to be spatially dispersive. Typically, this response is inherently weak, $|\varepsilon_{nl}(\boldsymbol{\kappa})| << |\varepsilon_{local}|$, but the impact on the overall wave dynamics can be emphasized in the limit in which the local response vanishes $\varepsilon_{local} \to 0$ (refs 94,95). Even more importantly, different structures exhibiting near-zero parameters, for example, wire media and multilayered metamaterials (see Box 1), are also known to exhibit a particularly strong non-local response and are inherently anisotropic. These result in exotic effects such as optical topological transitions at the ENZ frequency, where the isofrequency surface evolves from a closed ellipsoid to an open hyperboloid[96]. These and other related phenomena, often referred to as hyperbolic metamaterials[97,98], represent an interesting field in their own right and lie out of the scope of this Review. Here, we would simply remark that while anisotropy and enhanced spatial dispersion were traditionally considered constraints in the development of artificial electromagnetic media, they can also be exploited in numerous applications, including all-angle negative refraction[99–102] and imaging with subwavelength resolution[103–108]. Indeed, this strategy has led to several innovations, including hyperlenses[103–106] and canalization[107,108] approaches.

In summary, non-reciprocal, anisotropic, bianisotropic and non-local responses of matter are exceptionally strong and wealthy in structures with near-zero parameters. While previous works convey a number of effects of exceptional character, it can also be concluded that a complete and systematic study of all possible combinations of non-reciprocal, bianisotropic and non-local responses with structures with near-zero parameters has not yet been fully carried out and explored.

Outlook

Structures with near-zero parameters first attracted the attention of researchers as pathological cases in the field of metamaterials. Subsequent research discovered a number of unusual wave phenomena that challenged our understanding of light–matter interactions. Examples presented here have shown that near-zero refractive index photonics exhibits very distinctive features in basic light–matter interaction processes including the propagation, scattering, emission and confinement of light. Even more importantly, near-zero refractive index photonics also enables wave phenomena, such as tunnelling/supercoupling and geometry-invariant eigenmodes, which are exclusive to structures with near-zero parameters.

Over the next years, we expect that work on near-zero constitutive parameters may lead to innovative devices and trigger fundamental research in different subfields of optics. At this point, nonlinear optics, flexible photonics, quantum information processing and heat management seem to be some of the most promising areas. Ultimately, their technological impact will be determined by our ability to develop high-quality and, in particular, low-loss structures with near-zero parameters. In this quest, three major platforms may be the basis of a promising future: (1) the relatively low-loss polaritonic materials with an ENZ response in the thermal infrared; (2) CMOS-compatible and tunable semiconductor-based ENZ materials at near-infrared frequencies; and (3) low-loss all-dielectric metamaterial-based EMNZ media at optical frequencies. Together, they provide a basis from which to explore the technological and scientific potential of structures with near-zero parameters.

Methods

Methods and any associated references are available in the online version of the paper.

Received 17 September 2016; accepted 12 January 2017; published online 1 March 2017; corrected after print 6 March 2017

References

1. Engheta, N. & Ziolkowski, R. W. *Metamaterials: Physics and Engineering Explorations* (Wiley, 2006).
2. Eleftheriades, G. V. & Balmain, K. G. *Negative-Refraction Metamaterials: Fundamental Principles and Applications* (Wiley, 2005).
3. Cai, W. & Shalaev, V. M. *Optical Metamaterials: Fundamentals and Applications* (Springer, 2010).
4. Ziolkowski, R. W. Propagation in and scattering from a matched metamaterial having a zero index of refraction. *Phys. Rev. E* **70,** 046608 (2004).
5. Silveirinha, M. G. & Engheta, N. Tunneling of electromagnetic energy through subwavelength channels and bends using ε-near-zero materials. *Phys. Rev. Lett.* **97,** 157403 (2006).
6. Engheta, N. Pursuing near-zero response. *Science* **340,** 286–287 (2013).
7. Enoch, S., Tayeb, G., Sabouroux, P., Guérin, N. & Vincent, P. A metamaterial for directive emission. *Phys. Rev. Lett.* **89,** 213902 (2002).
8. Graciá-Salgado, R., García-Chocano, V. M., Torrent, D. & Sánchez-Dehesa, J. Negative mass density and ρ-near-zero quasi-two-dimensional metamaterials: design and applications. *Phys. Rev. B* **88,** 224305 (2013).
9. Wei, Q., Cheng, Y. & Liu, X. J. Acoustic total transmission and total reflection in zero-index metamaterials with defects. *Appl. Phys. Lett.* **102,** 174104 (2013).
10. Fleury, R. & Alù, A. Extraordinary sound transmission through density-near-zero ultranarrow channels. *Phys. Rev. Lett.* **111,** 055501 (2013).
11. Gu, Y., Cheng, Y., Wang, J. & Liu, X. Controlling sound transmission with density-near-zero acoustic membrane network. *J. Appl. Phys.* **118,** 024505 (2015).
12. Silveirinha, M. G. & Engheta, N. Metamaterial-inspired model for electron waves in bulk semiconductors. *Phys. Rev. B* **86,** 245302 (2012).
13. Silveirinha, M. G. & Engheta, N. Spatial delocalization and perfect tunneling of matter waves: electron perfect lens. *Phys. Rev. Lett.* **110,** 213902 (2013).
14. Fleury, R. & Alù, A. Manipulation of electron flow using near-zero index semiconductor metamaterials. *Phys. Rev. B* **90,** 035138 (2014).
15. Silveirinha, M. G. & Engheta, N. Theory of supercoupling, squeezing wave energy, and field confinement in narrow channels and tight bends using ε near-zero metamaterials. *Phys. Rev. B* **76,** 245109 (2007).
16. Edwards, B., Alù, A., Young, M. E., Silveirinha, M. G. & Engheta, N. Experimental verification of epsilon-near-zero metamaterial coupling and energy squeezing using a microwave waveguide. *Phys. Rev. Lett.* **100,** 033903 (2008).
17. Edwards, B., Alù, A., Silveirinha, M. G. & Engheta, N. Reflectionless sharp bends and corners in waveguides using epsilon-near-zero effects. *J. Appl. Phys.* **105,** 044905 (2009).
18. Alù, A., Silveirinha, M. G. & Engheta, N. Transmission-line analysis of ε-near-zero-filled narrow channels. *Phys. Rev. E* **78,** 016604 (2008).
19. Marcos, J. S., Silveirinha, M. G. & Engheta, N. μ-near-zero supercoupling. *Phys. Rev. B* **91,** 195112 (2015).
20. Mahmoud, A. M. & Engheta, N. Wave–matter interactions in epsilon-and-mu-near-zero structures. *Nat. Commun.* **5,** 5638 (2014).
21. Silveirinha, M. G. & Engheta, N. Design of matched zero-index metamaterials using nonmagnetic inclusions in epsilon-near-zero media. *Phys. Rev. B* **75,** 075119 (2007).

22. Huang, X., Lai, Y., Hang, Z. H., Zheng, H. & Chan, C. T. Dirac cones induced by accidental degeneracy in photonic crystals and zero-refractive-index materials. *Nat. Mater.* **10,** 582–586 (2011).
23. Nguyen, V. C., Chen, L. & Halterman, K. Total transmission and total reflection by zero index metamaterials with defects. *Phys. Rev. Lett.* **105,** 233908 (2010).
24. Hao, J., Yan, W. & Qiu, M. Super-reflection and cloaking based on zero index metamaterial. *Appl. Phys. Lett.* **96,** 101109 (2010).
25. Alù, A., Silveirinha, M. G., Salandrino, A. & Engheta, N. Epsilon-near-zero metamaterials and electromagnetic sources: tailoring the radiation phase pattern. *Phys. Rev. B* **75,** 155410 (2007).
26. Navarro-Cía, M., Beruete, M., Campillo, I. & Sorolla, M. Enhanced lens by ε and μ near-zero metamaterial boosted by extraordinary optical transmission. *Phys. Rev. B* **83,** 115112 (2011).
27. Navarro-Cía, M., Beruete, M., Sorolla, M. & Engheta, N. Lensing system and Fourier transformation using epsilon-near-zero metamaterials. *Phys. Rev. B* **86,** 165130 (2012).
28. Torres, V. *et al.* Experimental demonstration of a millimeter-wave metallic ENZ lens based on the energy squeezing principle. *IEEE Trans. Antennas Propag.* **63,** 231–239 (2015).
29. Pacheco-Peña, V. *et al.* Mechanical 144 GHz beam steering with all-metallic epsilon-near-zero lens antenna. *Appl. Phys. Lett.* **105,** 243503 (2014).
30. Soric, J. C. & Alù, A. Longitudinally independent matching and arbitrary wave patterning using ε-near-zero channels. *IEEE Trans. Microw. Theory Tech.* **63,** 3558–3567 (2015).
31. Alù, A. & Engheta, N. Boosting molecular fluorescence with a plasmonic nanolauncher. *Phys. Rev. Lett.* **103,** 043902 (2009).
32. Fleury, R. & Alù, A. Enhanced superradiance in epsilon-near-zero plasmonic channels. *Phys. Rev. B* **87,** 201101 (2013).
33. Sokhoyan, R. & Atwater, H. A. Quantum optical properties of a dipole emitter coupled to an ε-near-zero nanoscale waveguide. *Opt. Express* **21,** 32279–32290 (2013).
34. Sokhoyan, R. & Atwater, H. A. Cooperative behavior of quantum dipole emitters coupled to a zero-index nanoscale waveguide. Preprint at http://arxiv.org/abs/1510.07071 (2015).
35. Liberal, I. & Engheta, N. Nonradiating and radiating modes excited by quantum emitters in open epsilon-near-zero cavities. *Sci. Adv.* **2,** e1600987 (2016).
36. Vesseur, E. J. R., Coenen, T., Caglayan, H., Engheta, N. & Polman, A. Experimental verification of $n = 0$ structures for visible light. *Phys. Rev. Lett.* **110,** 013902 (2013).
37. Alù, A. & Engheta, N. Coaxial-to-waveguide matching with ε-near-zero ultranarrow channels and bends. *IEEE Trans. Antennas Propag.* **58,** 328–339 (2010).
38. Soric, J. C., Engheta, N., Maci, S. & Alù, A. Omnidirectional metamaterial antennas based on ε-near-zero channel matching. *IEEE Trans. Antennas Propag.* **61,** 33–44 (2013).
39. Shahmoon, E. & Kurizki, G. Nonradiative interaction and entanglement between distant atoms. *Phys. Rev. A* **87,** 033831 (2013).
40. Engheta, N., Salandrino, A. & Alù, A. Circuit elements at optical frequencies: nanoinductors, nanocapacitors, and nanoresistors. *Phys. Rev. Lett.* **95,** 095504 (2005).
41. Engheta, N. Circuits with light at nanoscales: optical nanocircuits inspired by metamaterials. *Science* **317,** 1698–1702 (2007).
42. Alù, A. & Engheta, N. All optical metamaterial circuit board at the nanoscale. *Phys. Rev. Lett.* **103,** 143902 (2009).
43. Alù, A. & Engheta, N. Optical 'shorting wires'. *Opt. Express* **15,** 13773–13782 (2007).
44. Edwards, B. & Engheta, N. Experimental verification of displacement-current conduits in metamaterials-inspired optical circuitry. *Phys. Rev. Lett.* **108,** 193902 (2012).
45. Li, Y., Liberal, I., Della Giovampaola, C. & Engheta, N. Waveguide metatronics: lumped circuitry based on structural dispersion. *Sci. Adv.* **2,** e1501790 (2016).
46. Liu, R., Roberts, C. M., Zhong, Y., Podolskiy, V. A. & Wasserman, D. Epsilon-near-zero photonics wires. *ACS Photon.* **3,** 1045–1052 (2016).
47. Rodríguez-Fortuño, F. J., Vakil, A. & Engheta, N. Electric levitation using epsilon-near-zero metamaterials. *Phys. Rev. Lett.* **112,** 033902 (2014).
48. Lindell, I. V & Sihvola, A. H. Electromagnetic boundary and its realization with anisotropic metamaterial. *Phys. Rev. E* **79,** 026604 (2009).
49. Rumsey, V. Some new forms of Huygens' principle. *IRE Trans. Antennas Propag.* **7,** 103–116 (1959).
50. Yaghjian, A. D. & Maci, S. Alternative derivation of electromagnetic cloaks and concentrators. *New J. Phys.* **10,** 115022 (2008).
51. von Neumann, J. & Wigner, E. *Über merkwürdige diskrete eigenwerte. Phys. Z.* **30,** 465–467 (1929).
52. Capasso, F. *et al.* Observation of an electronic bound state above a potential well. *Nature* **358,** 565–567 (1992).
53. Devaney, A. J. & Wolf, E. Radiating and nonradiating classical current distributions and the fields they generate. *Phys. Rev. D* **8,** 1044–1047 (1973).
54. Marengo, E. A. & Ziolkowski, R. W. On the radiating and nonradiating components of scalar, electromagnetic and weak gravitational sources. *Phys. Rev. Lett.* **83,** 3345–3349 (1999).
55. Marinica, D. C., Borisov, A. G. & Shabanov, S. V. Bound states in the continuum in photonics. *Phys. Rev. Lett.* **100,** 183902 (2008).
56. Lee, J. *et al.* Observation and differentiation of unique high-Q optical resonances near zero wave vector in macroscopic photonic crystal slabs. *Phys. Rev. Lett.* **109,** 067401 (2012).
57. Erentok, A. & Ziolkowski, R. W. A hybrid optimization method to analyze metamaterial-based electrically small antennas. *IEEE Trans. Antennas Propag.* **55,** 731–741 (2007).
58. Silveirinha, M. G. Trapping light in open plasmonic nanostructures. *Phys. Rev. A* **89,** 023813 (2014).
59. Monticone, F. & Alù, A. Embedded photonic eigenvalues in 3D nanostructures. *Phys. Rev. Lett.* **112,** 213903 (2014).
60. Lannebère, S. & Silveirinha, M. G. Optical meta-atom for localization of light with quantized energy. *Nat. Commun.* **6,** 8766 (2015).
61. Liberal, I., Mahmoud, A. M. & Engheta, N. Geometry-invariant resonant cavities. *Nat. Commun.* **7,** 10989 (2016).
62. Boyd, R. W. *Nonlinear Optics* (Academic, 2003).
63. Shen, Y. R. *The Principles of Nonlinear Optics* (Wiley, 1984).
64. Suchowski, H. *et al.* Phase mismatch—free nonlinear propagation in optical zero-index materials. *Science* **342,** 1223–1226 (2013).
65. Mattiucci, N., Bloemer, M. J. & D'Aguanno, G. Phase-matched second harmonic generation at the Dirac point of a 2-D photonic crystal. *Opt. Express* **22,** 6381–6390 (2014).
66. Powell, D. A. *et al.* Nonlinear control of tunneling through an epsilon-near-zero channel. *Phys. Rev. B* **79,** 245135 (2009).
67. Argyropoulos, C., Chen, P. Y., D'Aguanno, G., Engheta, N. & Alù, A. Boosting optical nonlinearities in ε-near-zero plasmonic channels. *Phys. Rev. B* **85,** 045129 (2012).
68. Argyropoulos, C., D'Aguanno, G. & Alù, A. Giant second-harmonic generation efficiency and ideal phase matching with a double ε-near-zero cross-slit metamaterial. *Phys. Rev. B* **89,** 235401 (2014).
69. Capretti, A., Wang, Y., Engheta, N. & Dal Negro, L. Enhanced third-harmonic generation in Si-compatible epsilon-near-zero indium tin oxide nanolayers. *Opt. Lett.* **40,** 1500–1503 (2015).
70. Capretti, A., Wang, Y., Engheta, N. & Dal Negro, L. Comparative study of second-harmonic generation from epsilon-near-zero indium tin oxide and titanium nitride nanolayers excited in the near-infrared spectral range. *ACS Photon.* **2,** 1584–1591 (2015).
71. Alam, M. Z., De Leon, I. & Boyd, R. W. Large optical nonlinearity of indium tin oxide in its epsilon-near-zero region. *Science* **352,** 795–797 (2016).
72. Caspani, L. *et al.* Enhanced nonlinear refractive index in ε-near-zero materials. *Phys. Rev. Lett.* **116,** 233901 (2016).
73. Vincenti, M. A., De Ceglia, D., Ciattoni, A. & Scalora, M. Singularity-driven second- and third-harmonic generation at epsilon-near-zero crossing points. *Phys. Rev. A* **84,** 063826 (2011).
74. Vassant, S., Hugonin, J.-P., Marquier, F. & Greffet, J.-J. Berreman mode and epsilon near zero mode. *Opt. Express* **20,** 23971–23977 (2012).
75. Vassant, S. *et al.* Epsilon-near-zero mode for active optoelectronic devices. *Phys. Rev. Lett.* **109,** 237401 (2012).
76. Campione, S., Brener, I. & Marquier, F. Theory of epsilon-near-zero modes in ultrathin films. *Phys. Rev. B* **91,** 121408(R) (2015).
77. Jun, Y. C. *et al.* Epsilon-near-zero strong coupling in metamaterial–semiconductor hybrid structures. *Nano Lett.* **13,** 5391–5396 (2013).
78. Campione, S. *et al.* Epsilon-near-zero modes for tailored light–matter interaction. *Phys. Rev. Appl.* **4,** 044011 (2015).
79. Molesky, S., Dewalt, C. J. & Jacob, Z. High temperature epsilon-near-zero and epsilon-near-pole metamaterial emitters for thermophotovoltaics. *Opt. Express* **21,** A96–A110 (2013).
80. Ciattoni, A., Marini, A., Rizza, C., Scalora, M. & Biancalana, F. Polariton excitation in epsilon-near-zero slabs: transient trapping of slow light. *Phys. Rev. A* **87,** 053853 (2013).
81. Ciattoni, A., Rizza, C. & Palange, E. Extreme nonlinear electrodynamics in metamaterials with very small linear dielectric permittivity. *Phys. Rev. A* **81,** 043839 (2010).
82. Krauss, T. F. Why do we need slow light? *Nat. Photon.* **2,** 448–450 (2008).
83. Boyd, R. W. Slow and fast light: fundamentals and applications. *J. Mod. Opt.* **56,** 1908–1915 (2009).
84. Rizza, C., Ciattoni, A. & Palange, E. Two-peaked and flat-top perfect bright solitons in nonlinear metamaterials with epsilon near zero. *Phys. Rev. A* **83,** 053805 (2011).
85. Marini, A. & Garcia de Abajo, F. J. Self-organization of frozen light in near-zero-index media with cubic nonlinearity. *Sci. Rep.* **6,** 20088 (2016).
86. Tretyakov, S. A., Nefedov, I. S., Sihvola, A. H., Maslovski, S. & Simovski, C. R. Waves and energy in chiral nihility. *J. Electromagn. Waves Appl.* **17,** 695–706 (2003).

87. Davoyan, A. R. & Engheta, N. Theory of wave propagation in magnetized near-zero-epsilon metamaterials: evidence for one-way photonic states and magnetically switched transparency and opacity. *Phys. Rev. Lett.* **111,** 257401 (2013).
88. Haldane, F. & Raghu, S. Possible realization of directional optical waveguides in photonic crystals with broken time-reversal symmetry. *Phys. Rev. Lett.* **100,** 013904 (2008).
89. Wang, Z., Chong, Y., Joannopoulos, J. D. & Soljačić, M. Observation of unidirectional backscattering-immune topological electromagnetic states. *Nature* **461,** 772–775 (2009).
90. Rechtsman, M. C. *et al.* Photonic floquet topological insulators. *Nature* **496,** 196–200 (2013).
91. Lumer, Y., Plotnik, Y., Rechtsman, M. C. & Segev, M. Self-localized states in photonic topological insulators. *Phys. Rev. Lett.* **111,** 243905 (2013).
92. Lu, L., Joannopoulos, J. D. & Soljačić, M. Topological photonics. *Nat. Photon.* **8,** 821–829 (2014).
93. Davoyan, A. R., Mahmoud, A. & Engheta, N. Optical isolation with epsilon-near-zero metamaterials. *Opt. Express* **21,** 3279–3286 (2013).
94. Belov, P. A. *et al.* Strong spatial dispersion in wire media in the very large wavelength limit. *Phys. Rev. B* **67,** 113103 (2003).
95. Pollard, R. J. *et al.* Optical nonlocalities and additional waves in epsilon-near-zero metamaterials. *Phys. Rev. Lett.* **102,** 127405 (2009).
96. Krishnamoorthy, H. N. S., Jacob, Z., Narimanov, E. E., Kretzschmar, I. & Menon, V. M. Topological transitions in metamaterials. *Science* **336,** 205–209 (2012).
97. Smith, D. R., Schurig, D., Mock, J. J., Kolinko, P. & Rye, P. Partial focusing of radiation by a slab of indefinite media. *Appl. Phys. Lett.* **84,** 2244–2246 (2004).
98. Poddubny, A. N., Iorsh, I., Belov, P. A. & Kivshar, Y. Hyperbolic metamaterials. *Nat. Photon.* **7,** 958–967 (2013).
99. Hoffman, A. J. *et al.* Negative refraction in semiconductor metamaterials. *Nat. Mater.* **6,** 946–950 (2007).
100. Yao, J. *et al.* Optical negative refraction in bulk metamaterials of nanowires. *Science* **321,** 930 (2008).
101. Fang, A., Koschny, T. & Soukoulis, C. M. Optical anisotropic metamaterials: negative refraction and focusing. *Phys. Rev. B* **79,** 245127 (2009).
102. Liu, Y., Bartal, G. & Zhang, X. All-angle negative refraction and imaging in a bulk medium made of metallic nanowires in the visible region. *Opt. Express* **16,** 15439–15448 (2008).
103. Salandrino, A. & Engheta, N. Far-field subdiffraction optical microscopy using metamaterial crystals: theory and simulations. *Phys. Rev. B* **74,** 075103 (2006).
104. Jacob, Z., Alekseyev, L. V & Narimanov, E. E. Optical hyperlens: far-field imaging beyond the diffraction limit. *Opt. Express* **14,** 8247–8256 (2006).
105. Liu, Z., Lee, H., Xiong, Y., Sun, C. & Zhang, X. Far-field optical hyperlens magnifying sub-diffraction-limited objects. *Science* **315,** 1686 (2007).
106. Smolyaninov, I. I., Hung, Y. J. & Davis, C. C. Magnifying superlens in the visible frequency range. *Science* **315,** 1699–1701 (2007).
107. Belov, P. A., Simovski, C. R. & Ikonen, P. M. T. Canalization of subwavelength images by electromagnetic crystals. *Phys. Rev. B* **71,** 193105 (2005).
108. Belov, P. A., Hao, Y. & Sudhakaran, S. Subwavelength microwave imaging using an array of parallel conducting wires as a lens. *Phys. Rev. B* **73,** 033108 (2006).
109. Anderegg, M., Feuerbacher, B. & Fitton, B. Optically excited longitudinal plasmons in potassium. *Phys. Rev. Lett.* **27,** 1565–1568 (1971).
110. Spitzer, W. G., Kleinman, D. & Walsh, D. Infrared properties of hexagonal silicon carbide. *Phys. Rev.* **113,** 127–132 (1959).
111. Korobkin, D., Urzhumov, Y. & Shvets, G. Enhanced near-field resolution in midinfrared using metamaterials. *J. Opt. Soc. Am. B* **23,** 468–478 (2006).
112. Caldwell, J. D. *et al.* Low-loss, infrared and terahertz nanophotonics using surface phonon polaritons. *Nanophotonics* **4,** 44–68 (2015).
113. Kim, J. *et al.* Role of epsilon-near-zero substrates in the optical response of plasmonic antennas. *Optica* **3,** 339–346 (2016).
114. Naik, G. V., Kim, J. & Boltasseva, A. Oxides and nitrides as alternative plasmonic materials in the optical range. *Opt. Mater. Express* **1,** 1090–1099 (2011).
115. Naik, G. V., Shalaev, V. M. & Boltasseva, A. Alternative plasmonic materials: beyond gold and silver. *Adv. Mater.* **25,** 3264–3294 (2013).
116. Kinsey, N. *et al.* Epsilon-near-zero Al-doped ZnO for ultrafast switching at telecom wavelengths. *Optica* **2,** 616–622 (2015).
117. Ou, J. Y. *et al.* Ultraviolet and visible range plasmonics of a topological insulator. *Nat. Commun.* **5,** 5139 (2014).
118. Khurgin, J. B. How to deal with the loss in plasmonics and metamaterials. *Nat. Nanotech.* **10,** 2–6 (2015).
119. Brown, J. Artificial dielectrics having refractive indices less than unity. *Proc. IEEE* **100,** 51–62 (1953).
120. Rotman, W. Plasma simulation by artificial dielectrics and parallel-plate media. *IRE Trans. Antennas Propag.* **10,** 17–19 (1962).
121. King, R. J., Thiel, D. V. & Park, K. S. The synthesis of surface reactance using an artificial dielectric. *IEEE Trans. Antennas Propag.* **31,** 471–476 (1983).
122. Della Giovampaola, C. & Engheta, N. Plasmonics without negative dielectrics. *Phys. Rev. B* **93,** 195152 (2016).
123. Pendry, J. B., Holden, A. J., Stewart, W. J. & Youngs, I. Extremely low frequency plasmons in metallic mesostructures. *Phys. Rev. Lett.* **76,** 4773–4776 (1996).
124. Moses, C. A. & Engheta, N. Electromagnetic wave propagation in the wire medium: a complex medium with long thin inclusions. *Wave Motion* **34,** 301–317 (2001).
125. Belov, P. A., Tretyakov, S. A. & Viitanen, A. Dispersion and reflection properties of artificial media formed by regular lattices of ideally conducting wires. *J. Electromagn. Waves Appl.* **16,** 1153–1170 (2002).
126. Maslovski, S. I., Tretyakov, S. A. & Belov, P. A. Wire media with negative effective permittivity: a quasi-static model. *Microw. Opt. Technol. Lett.* **35,** 47–51 (2002).
127. Smith, D. R., Padilla, W. J., Vier, D. C., Nemat-Nasser, S. C. & Schultz, S. Composite medium with simultaneously negative permeability and permittivity. *Phys. Rev. Lett.* **84,** 184184 (2000).
128. Maas, R., Parsons, J., Engheta, N. & Polman, A. Experimental realization of an epsilon-near-zero metamaterial at visible wavelengths. *Nat. Photon.* **7,** 907–912 (2013).
129. Wu, Y., Li, J., Zhang, Z. Q. & Chan, C. T. Effective medium theory for magnetodielectric composites: beyond the long-wavelength limit. *Phys. Rev. B* **74,** 085111 (2006).
130. Moitra, P. *et al.* Realization of an all-dielectric zero-index optical metamaterial. *Nat. Photon.* **7,** 791–795 (2013).
131. Li, Y. *et al.* On-chip zero-index metamaterials. *Nat. Photon.* **9,** 738–742 (2015).
132. Li, J., Zhou, L., Chan, C. T. & Sheng, P. Photonic band gap from a stack of positive and negative index materials. *Phys. Rev. Lett.* **90,** 083901 (2003).
133. Zhou, L., Song, Z., Huang, X. & Chan, C. T. Physics of the zero-*n* photonic gap: fundamentals and latest developments. *Nanophotonics* **1,** 181–198 (2012).
134. Ziolkowski, R. W. & Heyman, E. Wave propagation in media having negative permittivity and permeability. *Phys. Rev. E* **64,** 056625 (2001).
135. Javani, M. H. & Stockman, M. I. Real and imaginary properties of epsilon-near-zero materials. *Phys. Rev. Lett.* **117,** 107404 (2016).

Acknowledgements

This work is supported in part by the US Air Force Office of Scientific Research (AFOSR) Multidisciplinary University Research Initiative (MURI) award no. FA9550-12-1-0488 and in part by the AFOSR MURI award no. FA9550-14-1-0389. The authors would also like to acknowledge partial support from the Vannevar Bush Faculty Fellowship programme sponsored by the Basic Research Office of the Assistant Secretary of Defense for Research and Engineering and funded by the Office of Naval Research through grant N00014-16-1-2029.

Additional information

Reprints and permissions information is available online at www.nature.com/reprints. Correspondence should be addressed to N.E.

Competing financial interests

The authors declare no competing financial interests.

Methods

All numerical simulations were carried out using the commercially available solver COMSOL Multiphysics and a tetrahedral mesh. Simulations of tunnelling effects in Fig. 1b,c were performed in a 2D geometry and with the frequency domain solver. The waveguides were enclosed within a PEC boundary condition and then excited via transverse electromagnetic (TEM) waveguide ports. The emission simulations in Fig. 2a were performed in a 2D geometry and with the frequency domain solver. In this case, the system was excited with an out-of-plane (z-oriented) current line, and the system was terminated with a circular scattering boundary condition to emulate the emission into an unbounded space. The analysis of the cavities studied in Fig. 2d was carried out by using the eigenfrequency solver. In particular, a 3D open cavity was immersed in a vacuum space, which is itself terminated into a spherical PEC layer to enable the eigenfrequency analysis of a closed system.

Erratum: Near-zero refractive index photonics

Iñigo Liberal and Nader Engheta

Nature Photonics **11,** 149–158 (2017); published online 1 March 2017; corrected after print 6 March 2017.

Owing to technical problems, this Review Article was published online later than the date given in the print version. The published date should read '1 March 2017', and is correct in the online versions.